PROCEEDINGS of the
24th International Congress on Acoustics

October 24 to 28, 2022 in Gyeongju, Korea

ABS-0907

Parametric pinna model for a realistic representation of listener-specific pinna geometry

Katharina POLLACK*, Florian PAUSCH, Piotr MAJDAK

Acoustics Research Institute, Austrian Academy of Sciences, Vienna, Austria

*katharina.pollack@oeaw.ac.at

ABSTRACT

Personalised binaural audio requires individual head-related transfer functions (HRTFs). Nowadays, it is feasible to compute HRTFs numerically from meshes of a listener's anatomy. These meshes require geometric details of the pinna which are difficult to capture and often corrupted by noise and outliers. The alignment of a high-resolution template geometry to the captured listener geometry seems to be a promising approach to deal with these corruptions. However, such an alignment represents a multi-dimensional optimisation problem. To tackle this, we describe a parametric pinna model which reduces the representation of a non-pathological human pinna geometry from a few thousand points in space to 144 parameter dimensions. The model was evaluated in the geometric and psychoacoustic domains in terms of the Hausdorff distance distribution and simulated localisation errors, respectively. When aligned with individual ground-truth meshes, the parametric pinna model was able to represent these meshes with a small geometric error. The predicted sound-localisation performance, using the aligned meshes as a basis for HRTF calculations, was similar to that of the corresponding listener. These results indicate that the proposed parametric pinna model represents a versatile tool to create human pinna meshes with a detailed geometry for the calculation of individual HRTFs.

Keywords: head-related transfer functions, binaural audio, numerical calculation, shape alignment

1 INTRODUCTION

The acquisition of individual head-related transfer functions (HRTFs) for plausible binaural reproduction has been subject of research for a few decades. Augmented reality and virtual reality (AR/VR) systems evolved into commercial products, requiring an easy solution for individual HRTF acquisition. Besides the possibility to obtain individual HRTFs via acoustic measurement systems [1], numerical calculation represents a promising easy-to-use acquisition method [2, 3].

In order to numerically calculate accurate HRTFs, a three-dimensional (3D) representation of a listener's geometry, i.e., a mesh, is essential. While the head, neck, and torso can be modelled by simpler geometric shapes, such as spheres and trapezoids [4, 2], the sampling of the pinna geometry must be accurate with an average edge length of 1 mm of the triangular elements, resulting in meshes consisting of thousands of vertices. Because of this high dimensionality, a substantial reduction of the number of dimensions in the parameteric representation of the pinna geometry is required [5, 6, 7].

Non-individual HRTFs can be personalised by spectrally warping them using the pinna height, which is an easily measurable parameter [8]. Altough this method improves the degree of personalisation, it does not fully achieve it, which motivates a refined parametric description. The pinna geometry has been parameterised by means of additional anthropometric features, such as pinna height and width, cavum conchae depth, and others [7, 9]. One problem with these parameterisations is that they do not facilitate an unambiguous synthesis of a complete 3D pinna. Because of the fast development of computer graphics and augmented reality systems in recent years, there have been advances towards a more complicated parametric description of a pinna, one of which is revised in this study.

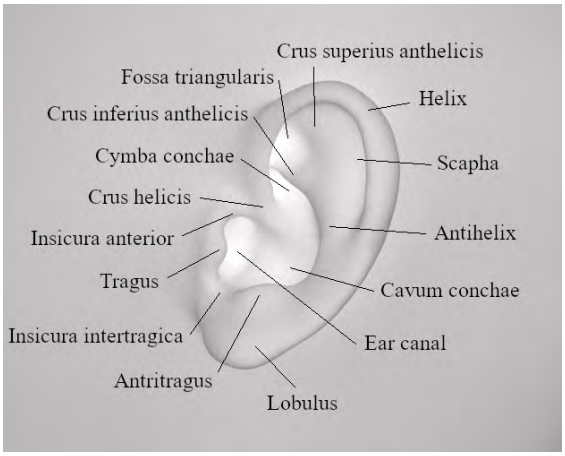

Figure 1. A human pinna including technical terms of various regions. The convex cavities, i.e., cymba and cavum conchae, fossa triangularis and scapha, are important for the first peaks and notches according to [10].

Figure 1 shows distinguished pinna regions, emphasizing that the pinna is a complex biological structure whose parametric description is not trivial. Based on this representation, one could use, e.g., these regions' prominences, i.e., depths, as parameters. In that case, the problem would be that these parameters are not easy to define for concave and convex areas uniformly and that they do not control the curvature of the corresponding or adjacent regions. Another approach would be to use a few carefully selected landmarks on the pinna surface that can be moved, with adjacent vertices of the mesh moving according to a proximity-based weighting. The problem with such an approach is that the pinna cavities cannot be deformed dramatically, as they do for human subjects (for example, the cavum conchae depth varies up to 30 % for inviduals [9]), and that the proximity cannot be defined as a sphere because of the small distance between structures. These approaches and their disadvantages demand a parametric representation that accounts for curvature and depth of the pinna geometry.

In this article, we describe a biologically motivated model of a pinna aiming at bridging the gap between a low-dimensional representation of a pinna geometry and an accurate pinna mesh for the calculation of individual HRTFs. We show that our model is capable of deforming a pinna mesh such that it approximates the pinnae of human subjects with a small geometric error, resulting in numerically calculated HRTFs showing similar sound-localisation errors as for highly accurate scans.

2 MODEL STRUCTURE

The concept of the described parametric pinna model (PPM) roots in skeletal animation and morph target animation, both concepts being usually applied in the area of animating digital characters, where the skeleton controlling the mesh is called "armature". Once the armature is constructed, it is attached to a template mesh such that changes in the armature deform the mesh globally and local regions of it. The armature consists of two elements: "bendy bones" and "control bones". Further, the PPM includes "shape keys" to fine-tune the geometry of the template mesh. Because the PPM is implemented in the graphics suite Blender (version 3.1.2)[1] [11], we use the software-specific terms.

2.1 Template mesh

The model's underlying pinna mesh is the average mesh of the WiDESPREaD database [12], which was derived from a geometric principal component analysis (PCA) performed on the left pinnae of 119 subjects. The subject meshes were acquired using a commercial structured-light-based scanner. This average pinna mesh will be denoted as $\mathbf{X}_0$ throughout the rest of this manuscript.

[1] http://www.blender.org

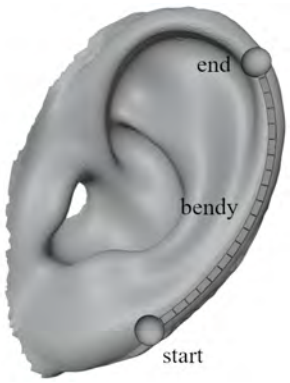

Figure 2. Example of one Bézier curve in the armature: bendy bone with two control bones (shown as spheres at the start and end of the bendy bone) following the curvature of the lower part of the helix. The displayed pinna mesh represents the template mesh $\mathbf{X}_0$.

2.2 Armature elements: Bézier curves

The armature is defined by cubic Bézier curves [13] $\mathbf{c}(l)$ along the surface of the pinna:

$$\mathbf{c}(l) = (1-l)^3\mathbf{p}_0 + 3(1-l)^2 l\mathbf{p}_1 + 3(1-l)l^2\mathbf{p}_2 + l^3\mathbf{p}_3, \tag{1}$$

with $0 \leq l \leq 1$, $l \in \mathbb{R}$, and $\mathbf{p}_q$, $q = \{0,1,2,3\}$, representing the curve's control points in 3D space. Points $\mathbf{p}_0$ and $\mathbf{p}_3$ correspond to the control points at the start and end of a Bézier curve, respectively. The rotation of the line between control points $\mathbf{p}_0$ and $\mathbf{p}_1$, and between control points $\mathbf{p}_2$ and $\mathbf{p}_3$ determines the amount of curve flexion. In the software interface, these relationships between the control points is simplified at the start and end of a Bézier curve with so-called "control bones" that are conveniently named "start" and "end", and the curve connecting the control bones is called "bendy bone". In our PPM, control bones can be translated and rotated, whereas bendy bones can be scaled in an isotropic way only. Figure 2 shows an example of such a bendy bone and its associated control bones.

The armature consists of nine Bézier curves, each with a bendy bone, and a start and end control bone. The armature additionally includes a special Bézier curve whose control points lie in line and whose control bones are not exposed in the model. This particular curve controls all bendy bones, allowing to globally translate, rotate, and scale the pinna mesh. In the PPM, we call this Bézier curve "parent bone", because it's a parent object in the software. The parent bone is the only one that may be scaled in an anisotropic way, while anisotropic scaling of bendy bones is not necessary to accurately describe a pinna mesh. In fact, because we do not need all degrees of freedom the software offers, not all parameter dimensions are exposed. The exposed parameters are rotation and translation of control bones, isotropic scaling of bendy bones, and rotation, translation and anistropic scaling of the parent bone. Table 1 gives an overview of the armature.

In order to fully control the pinna geometry, the armature is attached to the mesh by means of automated weighting. Automated weighting is implemented as a distance-based mapping of the amount of the rigid transformation of the armature, deforming the vertices in proximity of the corresponding bone. Slight changes to the weighting function were made manually to avoid overlap of adjacent regions of the complex geometry. Figure 3 shows the uniform weighting of the parent bone, and two examples of the mesh weighting for selected bendy bones.

The pinna mesh deformation $\Delta\mathbf{X}_\mathrm{b}$ as per armature modifications is described by

$$\Delta\mathbf{X}_\mathrm{b} = \sum_{i=1}^{M} \mathbf{A}_\mathrm{i}\left(\mathbf{X}_0, \mathbf{p}_\mathrm{q}\right), \tag{2}$$

where $M = 10$ is the number of all Bézier curves (consisting of bendy and control bones), and $\mathbf{A}_\mathrm{i}$ is a surjective function $f : \mathbb{R}^3 \mapsto \mathbb{R}^3$ that maps the parameter space to the mesh space. The function depends on $\mathbf{X}_0$, i.e., the

Table 1. List of the Bézier curves in our parametric pinna model. The first nine entries consist of the exposed parameters of a Bézier curve described by two control bones and a bendy bone, controlled by 13 parameters each. The tenth entry is the parent bone, controlled by 9 parameters.

Index	Name
1	Lobulus
2	Helix low
3	Helix middle
4	Helix up
5	Tragus
6	Antitragus
7	Antithelix
8	Crus inferius anthelicis
9	Crus superius anthelicis
10	Parent bone

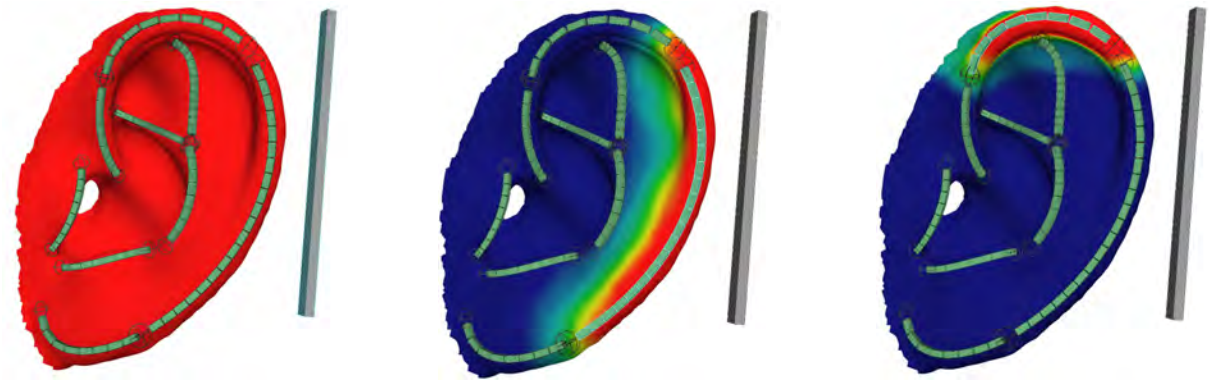

(a) (b) (c)

Figure 3. (a) Uniform weighting of the parent bone. (b, c) two bendy bones, ranging from none (blue) to maximum deformation (red). Note the overlap between the two weighting functions at the top of the helix.

(a) (b) (c)

Figure 4. (a) The armature of the PPM (green) attached to the template mesh. (b) Example translating and rotating the lower-helix control bones, and scaling of the corresponding bendy bone. (c) Resulting deformed template pinna, with hidden armature.

template mesh, and the parameter settings $\mathbf{p}_\mathrm{q}$ for the i-th Bézier curve. These parameters, i.e., the position of the control points of the Bézier curve in 3D space, are controlled in the model by rotating and translating control bones, isotropically scaling bendy bones, and rotating, translating and anisotropically scaling the parent bone.

Figure 4 displays the complete armature of the model and demonstrates a deformation of the helix as an example. Note that there are no points of discontinuity, and that the mesh is deformed in a smooth way.

2.3 Shape keys

Spatially less extensive changes of pinna areas are controlled via shape keys. Shape keys are described as a weighted deformation of the mesh:

$$\Delta\mathbf{X}_\mathrm{s} = \sum_{j=1}^{N} w_\mathrm{j}\mathbf{B}_\mathrm{j}, \tag{3}$$

where $\Delta\mathbf{X}_\mathrm{s}$ is the resulting mesh deformation, N describes the number of shape keys, $\mathbf{B}_\mathrm{j}$ describes the mesh deformation by the j-th shape key, and w_j the weights controlling the prominence of the corresponding shape-key deformation. Table 2 presents the weight ranges for each of the shape keys within our PPM.

2.4 Full model

The superposition of Eq. (2) and (3) yields the complete equation describing the deformed mesh controlled by the parameters of the PPM:

$$\mathbf{X}_\mathrm{PPM} = \underbrace{\mathbf{X}_0}_{\text{template}} + \underbrace{\Delta\mathbf{X}_\mathrm{b}}_{\text{bones}} + \underbrace{\Delta\mathbf{X}_\mathrm{s}}_{\text{shape keys}} = \mathbf{X}_0 + \sum_{i=1}^{M}\mathbf{A}_\mathrm{i}\left(\mathbf{X}_0, \mathbf{p}_\mathrm{q}\right) + \sum_{j=1}^{N} w_\mathrm{j}\mathbf{B}_\mathrm{j}, \tag{4}$$

with $M = 10$ Bézier curves and $N = 18$ shape keys. As for the total number of dimensions, we have nine degrees of freedom (DOFs) for the parent bone (translation, rotation, anistropic scaling), six DOFs for each control bone (translation and rotation), one DOF for each bendy bone (isotropic scaling), and one DOF for each shape key (weights w_j), resulting in a total of 144 dimensions:

$$\dim\{\mathbf{X}_\mathrm{PPM}\} = \underbrace{6+3}_{\text{parent bone}} + \underbrace{(M-1)\cdot 1}_{\text{bendy bones}} + \underbrace{2\cdot(M-1)\cdot 6}_{\text{control bones}} + \underbrace{N}_{\text{shape keys}} = 144. \tag{5}$$

Table 2. Shape keys and corresponding weight ranges available in our parametric pinna model.

Index	Shape-key name	Weight ranges
1	Antitragus-Crease	$-1 \leq w_1 \leq 1$
2	Cavum_conchae-Depth	$-1 \leq w_2 \leq 1$
3	Cymba_conchae-Depth	$0 \leq w_3 \leq 1$
4	Crus_helicis-Prominence	$-1 \leq w_4 \leq 1$
5	Upper_helix-Depth	$0 \leq w_5 \leq 1$
6	Middle_helix-Depth	$0 \leq w_6 \leq 1$
7	Lower_helix-Depth	$0 \leq w_7 \leq 1$
8	Lobulus-Form	$0 \leq w_8 \leq 1$
9	Scapha-Depth	$0 \leq w_9 \leq 1$
10	Fossa_triangularis-Depth	$-1 \leq w_{10} \leq 1$
11	Crus_inferius_anthelicis-Lower_crease	$0 \leq w_{11} \leq 1$
12	Crus_inferius_anthelicis-Upper_crease	$0 \leq w_{12} \leq 1$
13	Crus_superius_anthelicis-Lower_crease	$0 \leq w_{13} \leq 1$
14	Crus_superius_anthelicis-Upper_crease	$0 \leq w_{14} \leq 1$
15	Tragus-Upper_dent	$-1 \leq w_{15} \leq 1$
16	Crus_helicis-Upper_dent	$0 \leq w_{16} \leq 1$
17	Crus_helicis-Lower_dent	$0 \leq w_{17} \leq 1$
18	Ear_canal-Diameter	$-1 \leq w_{18} \leq 1$

3 EVALUATION

We evaluated the model by aligning the template pinna to six target pinnae by manually deforming the described parametric pinna model. The target meshes were obtained from subjects of the databases maintained by the Acoustics Research Institute (ARI), Austria, and the Sorbonne University (SOU), France. To adequately sample the geometric space spanning possible non-pathological human pinnae, we chose six pinnae that have distinctive features. For example, NH1060 shows a wide scapha and a small lobulus, NH130 shows opposed values for these parameters. In order to explore the pinna dimensions and further develop the PPM, we exported the deviations from the default parameter values.

The alignment process was as follows: A target mesh of another pinna was loaded into the Blender workspace. First, the parent bone was used for globally setting the location, orientation and size of the PPM such that the template pinna roughly aligns with the target mesh. After that, the control bones and bendy bones were sequentially translated, rotated and scaled respectively until the deformed template pinna was aligned with the target pinna. In this step, we focused on high alignment accuracy in convex regions.

For further refinement of the alignment, the weights of the shape keys were adjusted to synthesize the concave target-pinna structures. Due to the overlapping weighting of the bendy bones and the manual definition of the shape keys, changing one parameter manipulates a region another, possibly multiple parameters influence as well. Thus, transforming the armature and adjusting shape key weights was done in an alternating fashion, representing an iterative process.

The alignment was completed once the mean geometric error between the deformed template pinna and the target mesh was below an a-priori defined error margin of 1 mm. Note that certain pinna regions needed to be aligned with particular care since larger errors may lead to perceivable effects when listening via the numerically calculated HRTF [7].

For all six subjects, ground truth meshes (coming from a computed tomography scan of a head cast [14]) were provided. These serve the evaluation for both the geometric and the psychoacoustic domain. It has been shown that these meshes provide the geometric accuracy necessary for the calculated HRTFs to yield similar sound-localisation errors as HRTFs from a measurement of the corresponding listener [14, 15]. In this evaluation, we thus only consider results from numerically calculated HRTFs.

In the geometric domain, the alignment process was evaluated using the distance between two point sets, i.e., the deformed template mesh and the target mesh. A metric commonly used in medical image processing is the Hausdorff distance [16], describing the largest smallest Euclidean distance between two meshes. However, this single-value metric does not sufficiently describe whether an alignment was successful or not. Thus, we used a point-wise single-sided Hausdorff distance, i.e., taking the smallest Euclidean distance for every point of the target pinna to the deformed template pinna, and inspect its distribution.

In the psychoacoustic domain, the alignment process was evaluated by means of sound-localisation errors, specifically quadrant error and polar error. We numerically calculated HRTFs from the ground-truth meshes, which were used as reference HRTFs for the evaluation in the psychoacoustic domain. After the alignment using our model, the left pinna was stitched back to the ground truth mesh and we calculated the HRTFs again. This way, we could ensure the only change between the HRTFs is the influence of the left pinna. The HRTFs were calculated using the the open-source software Mesh2HRTF v1.0[2]. Since the pinna is mostly responsible for elevation perception [17], we used the model predicting sound-localisation performance in sagittal planes [18], implemented as the function `baumgartner2014` from the Auditory Modeling Toolbox (AMT) v1.2[3][19]. This model simulates how a subject would perform in a localisation experiments given the ground-truth HRTFs as a reference versus the calculated HRTFs from the PPM-aligned mesh stitched to the ground-truth head mesh.

4 RESULTS

Figure 5 shows the range distribution of all PPM parameters for the six alignments as a function of deviation from the default state. Figure 6 shows the Euclidean distance distribution of the PPM-aligned mesh versus the target mesh, i.e., the ground truth, calculated and visualised with Meshlab [20][4]. All alignments resulted in geometric distance values largely below the one-millimeter threshold. It has been shown that an accuracy of distance values at approximately 1 mm lead to perceptually valid HRTFs by means of sound-localisation errors [14, 21].

Figure 7 shows the results of the sound-localisation model predictions, i.e., computed quadrant error rates and polar errors for the HRTFs resulting from five of the alignments. The sensitivities have been adapted such that the quadrant error of the reference is at approximately 8 % for each subject, according to [22]. In the psychoacoustic domain, we showed that the HRTFs from PPM-aligned meshes yield similar sound-localisation errors as HRTFs calculated from the the ground-truth meshes. The differences in the quadrant error for subjects NH1059, NH1060, and NH1061 can be explained by the geometric error in the fossa triangularis and cymba conchae for the bottom row in Fig. 6.

5 CONCLUSION

We revisited a recently proposed PPM and described its structure and key components in detail, focusing on the mathematical description connecting to the software-dependent terminology. In order to investigate model applicability for individualisation of HRTFs, the PPM was manually controlled to align the average mesh to six human target pinnae, and the deformed meshes were evaluated in the geometric and psychoacoustic domains. We showed that the PPM was able to approximate the target meshes with a geometric error largely below

[2] https://github.com/Any2HRTF/Mesh2HRTF
[3] https://amtoolbox.org/
[4] https://www.meshlab.net/

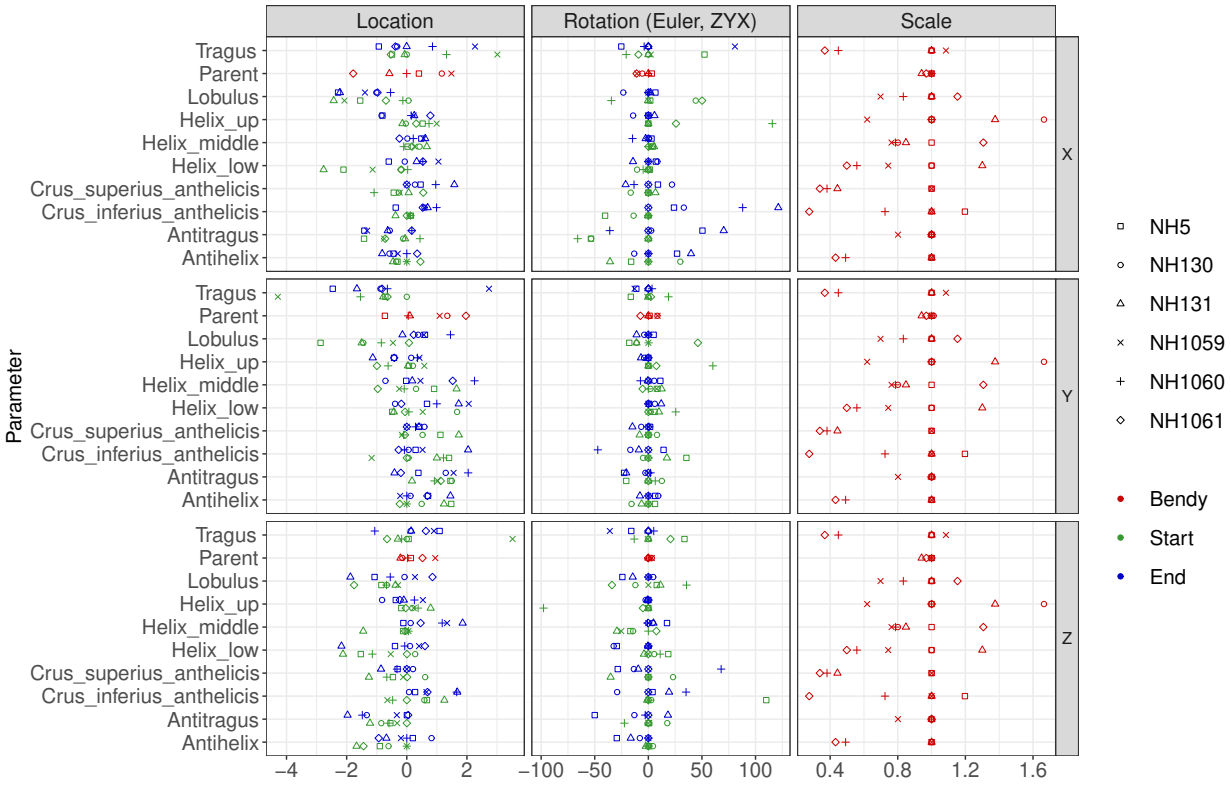

(a) Parent bone, bendy bones and control bones.

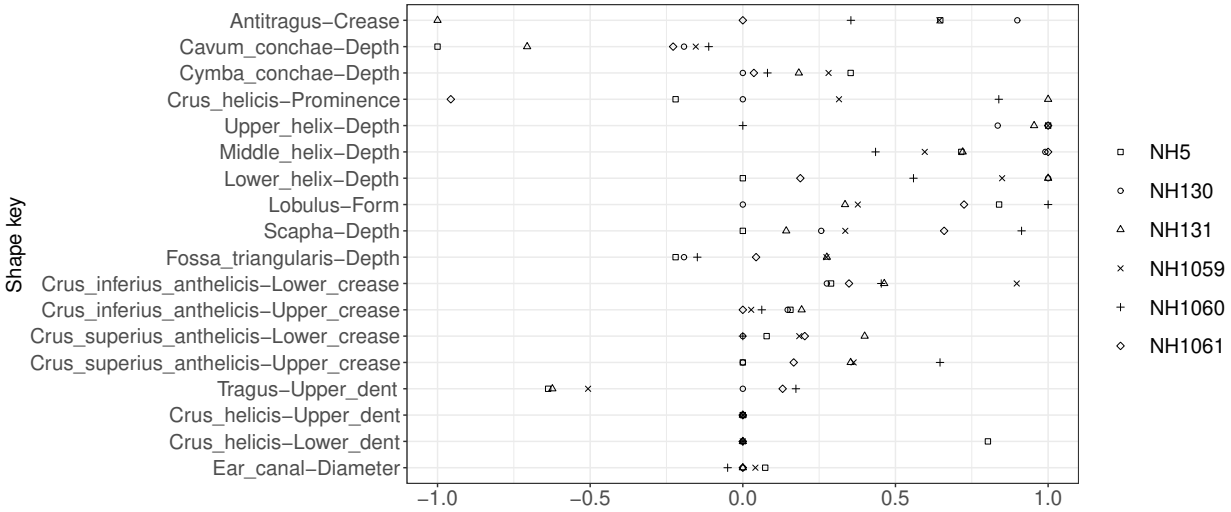

(b) Shape keys.

Figure 5. Parameter ranges of (a) the parent bone, bendy bones and control bones, and (b) the shape keys. Location and rotation are provided in mm and deg, respectively. Rotations are represented by Euler angles with axis-rotation order ZYX.

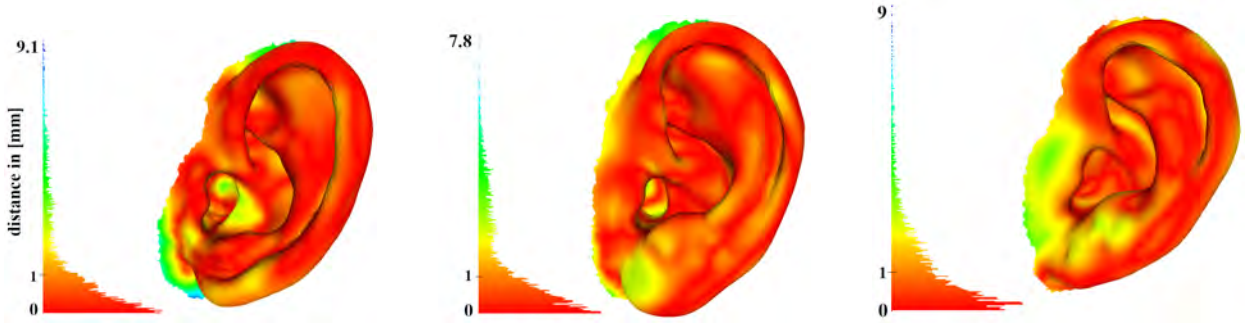

(a) NH5, 0.81 mm median distance (b) NH130, 0.72 mm median distance (c) NH131, 0.83 mm median distance

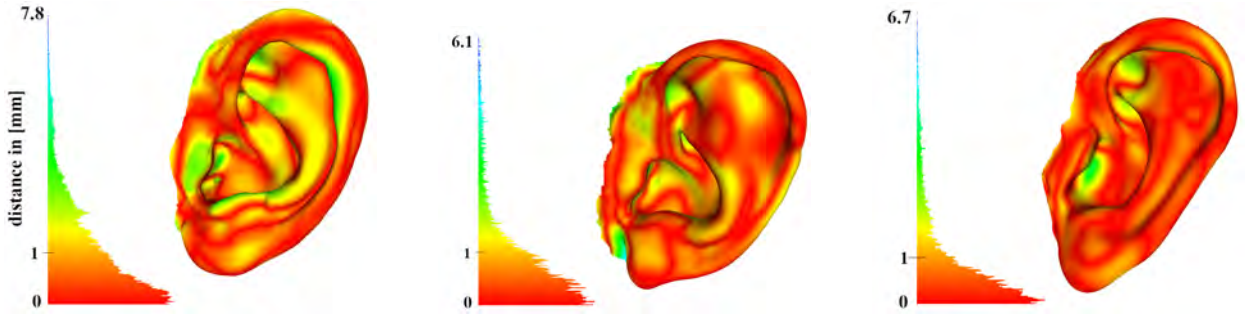

(d) NH1059, 1.04 mm median distance (e) NH1060, 0.72 mm median distance (f) NH1061, 0.59 mm median distance

Figure 6. Geometric error distribution between the PPM-aligned meshes and the corresponding ground truth mesh, for six different subjects. Left of the coloured pinnae are the individual distance distributions in mm, ranging from red (error at 1 mm or below) over green (error at approx. 3.5 mm) to blue (error over approx. 5 mm). Subcaptions indicate the median value of the corresponding distance distribution.

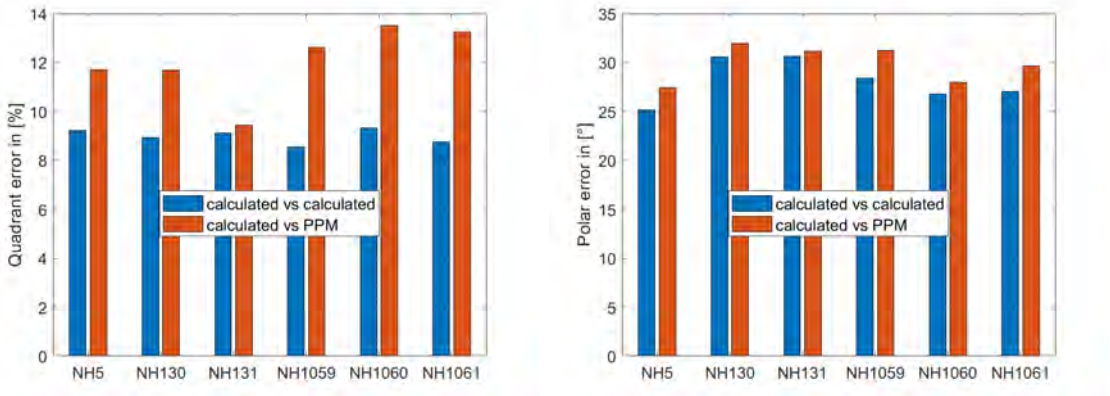

(a) (b)

Figure 7. (a) Quadrant-error rate in % and (b) polar error in deg.

1 mm. In the psychoacoustic domain, predictions of the saggital-plane sound-localisation performance were obtained based on the individual HRTFs, which were numerically calculated from the ground-truth meshes and PPM-aligned meshes. Compared to the results from the corresponding ground-truth HRTFs, both the geometric error and the predictions of the auditory model indicate that the PPM was able to accurately synthesize the considered human pinnae. With this geometric and psychoacoustic accuracy, it is likely that the HRTFs calculated from PPM-aligned meshes yield similar localisation errors as measured HRTFs in a physical sound-localisation experiment.

The pinna is a highly complex biological structure, and especially the cavities which geometric dimensions are difficult to describe are the important regions of the pinna responsible for peaks and notches in HRTFs. The problem of describing this structure is a multidimensional one, and it is not easy to solve. The proposed PPM serves as a bridge for the gap between a low-dimensional parametric pinna geometry description and high-accurate mesh synthesis.

For future applications, the model control will be improved to enable an automated alignment process, for which the exploration of the possible parameter ranges will help. But already in its current state, the model represents a versatile tool to achieve a parameteric description of the pinna geometry, facilitating access to individual HRTFs for a wide audience.

ACKNOWLEDGEMENTS

We thank Mantas Tamulionis for his contributions to the implementation of the PPM Matlab interface. The work of K.P. and P.M. was supported by the Austrian Research Promotion Agency (FFG, grant no. 871263, project "softpinna"). All authors received funding from the European Union's Horizon 2020 research and innovation funding programme (grant no. 101017743, project "SONICOM"–Transforming auditory-based social interaction and communication in AR/VR).

REFERENCES

[1] S. Li and J. Peissig, "Measurement of Head-Related Transfer Functions: A Review," *Applied Sciences*, vol. 10, p. 5014, Jan. 2020. Number: 14 Publisher: Multidisciplinary Digital Publishing Institute.

[2] K. Pollack, W. Kreuzer, and P. Majdak, "Modern acquisition of personalised head-related transfer functions: An overview," in *Advances in Fundamental and Applied Research on Spatial Audio* (D. B. F. Katz and D. P. Majdak, eds.), ch. 4, Rijeka: IntechOpen, 2022.

[3] W. Kreuzer, P. Majdak, and Z. Chen, "Fast multipole boundary element method to calculate head-related transfer functions for a wide frequency range," *The Journal of the Acoustical Society of America*, vol. 126, pp. 1280–1290, Sept. 2009.

[4] V. R. Algazi, R. O. Duda, R. Duraiswami, N. A. Gumerov, and Z. Tang, "Approximating the head-related transfer function using simple geometric models of the head and torso," *The Journal of the Acoustical Society of America*, vol. 112, no. 5, pp. 2053–2064, 2002.

[5] K. Pollack, F. Brinkmann, P. Majdak, and W. Kreuzer, "Von fotos zu personalisierter räumlicher audiowiedergabe," *e & i Elektrotechnik und Informationstechnik*, pp. 1–6, 2021.

[6] K. Pollack, P. Majdak, and H. Furtado, "A Parametric Pinna Model for the Calculations of Head-Related Transfer Functions," in *Proceedings of Forum Acusticum*, (Lyon), pp. 1357–1360, 2020.

[7] P. Stitt and B. F. G. Katz, "Sensitivity analysis of pinna morphology on head-related transfer functions simulated via a parametric pinna model," *The Journal of the Acoustical Society of America*, vol. 149, pp. 2559–2572, Apr. 2021.

[8] J. C. Middlebrooks, "Individual differences in external-ear transfer functions reduced by scaling in frequency," *The Journal of the Acoustical Society of America*, vol. 106, no. 3, pp. 1480–1492, 1999.

[9] V. R. Algazi, R. O. Duda, D. M. Thompson, and C. Avendano, "The CIPIC HRTF database," in *Proceedings of the 2001 IEEE Workshop on the Applications of Signal Processing to Audio and Acoustics (Cat. No.01TH8575)*, (New York), pp. 99–102, 2001.

[10] H. Takemoto, P. Mokhtari, H. Kato, R. Nishimura, and K. Iida, "Mechanism for generating peaks and notches of head-related transfer functions in the median plane," *The Journal of the Acoustical Society of America*, vol. 132, pp. 3832–41, Dec. 2012.

[11] B. O. Community, *Blender - a 3D modelling and rendering package*. Blender Foundation, Stichting Blender Foundation, Amsterdam, 2018.

[12] C. Guezenoc and R. Seguier, "A wide dataset of ear shapes and pinna-related transfer functions generated by random ear drawings," *The Journal of the Acoustical Society of America*, vol. 147, no. 6, pp. 4087–4096, 2020.

[13] P. E. Bézier and S. Sioussiou, "Semi-automatic system for defining free-form curves and surfaces," *Computer-Aided Design*, vol. 15, no. 2, pp. 65–72, 1983.

[14] H. Ziegelwanger, A. Reichinger, and P. Majdak, "Calculation of listener-specific head-related transfer functions: Effect of mesh quality," in *Proceedings of Meetings on Acoustics*, vol. 19, (Montreal, Canada), p. 050017, 2013.

[15] H. Ziegelwanger, P. Majdak, and W. Kreuzer, "Numerical calculation of listener-specific head-related transfer functions and sound localization: Microphone model and mesh discretization," *The Journal of the Acoustical Society of America*, vol. 138, pp. 208–222, July 2015.

[16] D. Pompeiu, "Sur la continuité des fonctions de variables complexes," in *Annales de la Faculté des sciences de Toulouse: Mathématiques*, vol. 7, pp. 265–315, 1905.

[17] D. W. Batteau, "The role of the pinna in human localization," *Proceedings of the Royal Society of London. Series B. Biological Sciences*, vol. 168, no. 1011, pp. 158–180, 1967.

[18] R. Baumgartner, P. Majdak, and B. Laback, "Modeling sound-source localization in sagittal planes for human listeners," *The Journal of the Acoustical Society of America*, vol. 136, no. 2, pp. 791–802, 2014.

[19] P. Majdak, C. Hollomey, and R. Baumgartner, "Amt 1. x: A toolbox for reproducible research in auditory modeling," *Acta Acustica*, vol. 6, p. 19, 2022.

[20] P. Cignoni, M. Callieri, M. Corsini, M. Dellepiane, F. Ganovelli, and G. Ranzuglia, "MeshLab: an Open-Source Mesh Processing Tool," in *Eurographics Italian Chapter Conference* (V. Scarano, R. D. Chiara, and U. Erra, eds.), pp. 129–136, The Eurographics Association, 2008.

[21] K. Pollack and P. Majdak, "Evaluation of a parametric pinna model for the calculation of head-related transfer functions," in *Immersive and 3D Audio (I3DA) conference*, 2021.

[22] J. C. Middlebrooks, "Virtual localization improved by scaling nonindividualized external-ear transfer functions in frequency," *The Journal of the Acoustical Society of America*, vol. 106, no. 3, pp. 1493–1510, 1999.